Front. Med. 2019, 13(5): 564–574
https://doi.org/10.1007/s11684-018-0676-2

RESEARCH ARTICLE

Deciphering the pharmacological mechanism of Guan-Jie-Kang in treating rat adjuvant-induced arthritis using omics analysis

Hudan Pan[1,*], Yanfang Zheng[1,2,*], Zhongqiu Liu[3], Zhongwen Yuan[1], Rutong Ren[1], Hua Zhou[1], Ying Xie (✉)[1], Liang Liu (✉)[1]

[1]*State Key Laboratory of Quality Research in Chinese Medicine/Macau Institute for Applied Research in Medicine and Health, Macau University of Science and Technology, Macau, China;* [2]*Fujian University of Traditional Chinese Medicine, Fuzhou 350122, China;* [3]*International Institute for Translational Research of Traditional Chinese Medicine of Guangzhou University of Chinese Medicine, Guangzhou 510006, China*

Abstract **Traditional Chinese medicine (TCM) formulas have attracted increasing attention worldwide in the past few years for treating complex disease including rheumatoid arthritis. However, their mechanisms are complex and remain unclear. Guan-Jie-Kang (GJK), a prescription modified from "Wu Tou Decoction," was found to significantly relieve arthritis symptoms in rats with adjuvant-induced arthritis after 30-day treatment, especially in the 24 g/kg/day group. By analyzing 1749 targets related to 358 compounds in the five herbs of GJK, we identified the possible anti-arthritis pathways of GJK, including the calcium signaling and metabolic pathways. Bone damage levels were assessed by micro-computed tomography, and greater bone protective effect was observed with GJK treatment than with methotrexate. Receptor activator of nuclear factor κB ligand (RANKL)–RANK signaling, which is related to calcium signaling, was significantly regulated by GJK. Moreover, a target metabolomics assay of serum was conducted; 17 metabolic biomarkers showed significant correlations with treatment. An integrated pathway analysis revealed that pyruvate metabolism, purine metabolism, and glycolysis metabolism were significantly associated with the effects of GJK in arthritis treatment. Thus, this study establishes a new omics analytical method integrated with bioinformatics analysis for elucidating the multi-pathway mechanisms of TCM.**

Keywords rheumatoid arthritis; traditional Chinese medicine; pharmacological mechanism; metabolism; adjuvant-induced arthritis; omics analysis

Introduction

Rheumatoid arthritis (RA) affects 0.5%–1% of the global population [1–3] and is a chronic, systemic autoimmune disease characterized by progressive disability, systemic complications, early death, and socioeconomic costs [4,5]. The treatments for RA have evolved in the past two decades with the advent of biological agents [6,7]. However, as RA is a complex, multi-target disease, biological agents do not provide complete symptom resolution: not all patients experience relief after full-course therapy, and symptom relief usually requires ongoing treatment [8–10]. Moreover, infectious diseases, especially hepatitis B and tuberculosis, and high costs restrict the prescription of biologics in China. Less than 10% of RA patients in China receive anti-tumor necrosis factor α (TNF-α) therapy [11,12].

Traditional Chinese medicines (TCMs) have been used to treat RA in China for a long time [13,14]. Recently, based on the development of new TCM research technologies, TCM has attracted increasing attention for the treatment of complex diseases, such as RA, because of its well-accepted "multi-components against multi-targets" [15] characteristic. Guan-Jie-Kang (GJK), a traditional Chinese herbal formula modified from the well-proven "Wu Tou Decoction" (WTD), has been used for many years in China. RA patients given GJK showed marked improvements in clinical symptoms and few side effects. A liquid chromatography–tandem mass spectrometry (LC-MS/MS) method has been developed to control the quality and stability of GJK [16].

However, determining the mechanisms of GJK is

Received July 19, 2018; accepted October 27, 2018

Correspondence: Liang Liu, lliu@must.edu.mo;
Ying Xie, yxie@must.edu.mo

*These authors contributed equally to this work.

difficult because of its diverse ingredients and complex interactions within the human body. Approaches using bioinformatics analysis tools, such as the Traditional Chinese Medicine Integrated Database (TCMID), allow the systematic study of the potential mechanisms of prescriptions based on networks composed of active ingredients and their targets [17–19].

Moreover, with the development of information-rich techniques, such as genomics, proteomics, and metabolomics, the molecular mechanisms of TCMs can be explored. Indeed, metabolomics has developed into the most useful omics technique for TCM studies because it facilitates visualizing complete organism pathways. However, both omics techniques and bioinformatics analyses have limitations in evaluating the "multi-component, multi-target, and multi-pathway" mechanisms of TCMs.

In this study, we explore the potential mechanisms of GJK in arthritis treatment in an experimental adjuvant-induced arthritis (AIA) model using both bioinformatics and metabolomics analyses. The study overview is presented in Fig. 1.

Methods

Animals

Sprague–Dawley rats (male, 110–130 g) were bought from the Guangdong Medical Laboratory Animal Center (Guangzhou, China). All procedures were approved by the Animal Ethical Council of Guangzhou University of Chinese Medicine.

Plant materials and extract preparation

GJK was prepared according to a previously described method [16,20]. In brief, the composition of GJK is Radix Astragali (10 g), Radix Glycyrrhizae (6 g), Radix Paeoniae Alba (12 g), Aconiti Lateralis Radix Praeparata (10 g), and Corydalis Rhizome (10 g). A total of 9.6 kg prescription (200 folds) was extracted twice with water in 95 °C. First, the prescription was extracted with ninefold amount of water for 1.5 h, and then fivefold amount of water was used to extract for 1 h. After combining the two extracts, we filtered the leaves and concentrated them at 60 °C. Finally, the extracts were obtained and stored at 4 °C for further experiments.

AIA in rats and treatment administration

All experimental procedures were strictly performed in accordance with the institutional guidelines for the care and use of laboratory animals in China. Adjuvant arthritis was induced rapidly by Complete Freund's Adjuvant (CFA) injection into the base of rat tails as described in our previous study [21]. The rats were randomly divided into five groups for oral administration: normal control group, AIA model, positive control (methotrexate (MTX), 7.6

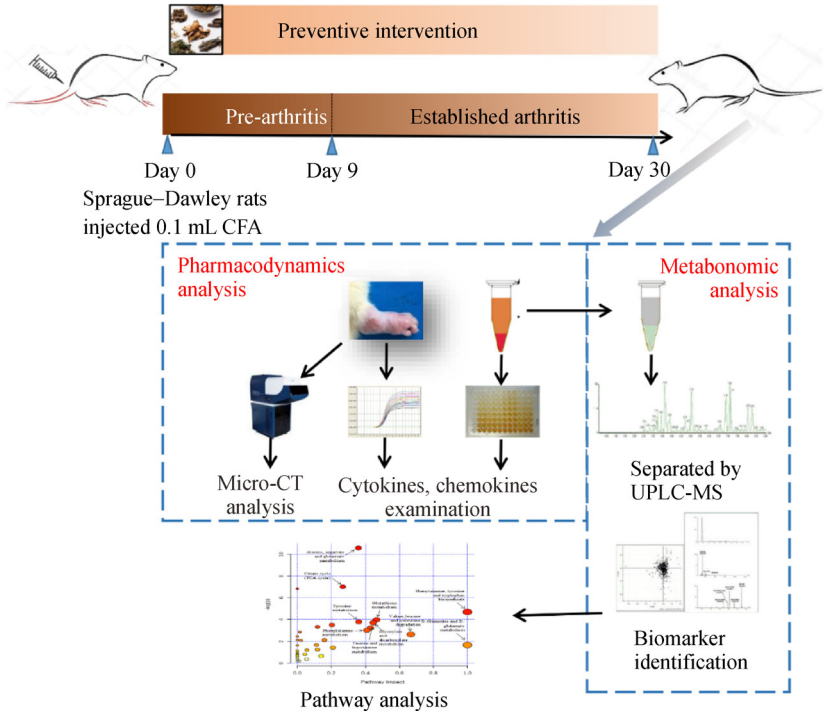

Fig. 1 Study overview.

mg/kg body weight per week), GJK (16 g crude herb/kg body weight per day), and GJK (24 g crude herb/kg body weight per day). Each group comprised 10–12 rats.

Assessment of AIA

The clinical symptoms of arthritis were evaluated based on increased hind paw volumes and arthritis scores by two independent observers. Both hind paw volumes were measured using a plethysmometer chamber (Yiyan Technology, Jinan, China) on days 0, 7, 10, 13, 16, 19, 22, 25, 28, and 30 after the induction of arthritis. Arthritis scores were evaluated concomitantly with paw volume assessments. Blood samples were collected from the abdominal aorta of narcotized rats on day 30. Then, the rats were killed by cervical dislocation. The erythrocyte sedimentation rate (ESR) was determined by a modified method based on International Council for Standardization in Haematology selected methods. Spleen and thymus indexes were calculated as the ratio (mg/g) of the organ wet weight versus the body weight [22].

Micro-computed tomography (micro-CT)

Ankles were fixed in 4% paraformaldehyde and 70% ethanol and then scanned using an *ex vivo* micro-CT scanner (Bruker, Kontich, Belgium). Scans were conducted using a voxel size of 35 μm, an X-ray tube current of 441 μA, and a voltage of 43 kV. The 3D micro-structural properties of the bone were evaluated using the CT Analyzer software (Bruker, Germany). Five indexes, including the trabecular bone mineral density (BMD), trabecular volume rate (BV/TV), trabecular number (Tb. N), porosity percentage, and tissue mineral density (TMD), were analyzed and appeared to change as arthritis developed. We modified and normalized the formula as follows: $(X-\min)/(\max-\min)$ or $1-(X-\min)/(\max-\min)$. Then, the five items were averaged to obtain the final micro-CT score reflecting all five bone parameters.

Cytokine expression test

The levels of interleukin (IL)-1β, TNF-α, IL-17, and IL-6 in serum were measured using commercially available enzyme-linked immunosorbent assay (ELISA) kits according to the manufacturer's instructions.

Real-time quantitative polymerase chain reaction (PCR) analysis

Total RNA was extracted with TRIzol reagent. Reverse transcriptase (Roche (Milwaukee, Wisconsin, United States)) was used according to the manufacturer's instructions for the synthesis of complementary DNA (cDNA). Real-time quantitative PCR was performed by applying the FastStart Universal SYBR Green Master Mix. cDNA was amplified with the following primers: for TNF-α, 5′-CGT GTT CAT CCG TTC TCT ACC-3′ and 5′-CCA CTC AGG CAT CGA CAT T-3′; for IL-1β, 5′-TCT CAC AGC AGC ATC TCG AC-3′ and 5′-GGT CGT CAT CAT CCC ACG AG-3′; for IL-17, 5′-GTT CAG TGT GTC CAA ACG CC-3′ and 5′-CAT TGC GGC TCA GAG TCC AG-3′; for IL-6, 5′-CTC TCC GCA AGA GAC TTC CAG-3′ and 5′-TTC TGA CAG TGC ATC ATC GCT-3′; for receptor activator of nuclear factor κ B ligand (RANKL), 5′-CAA CCG AGA CTA CGG CAA GT-3′ and 5′-TTA GGA TCC ATC TGC GCT CG-3′; for osteoprotegerin (OPG), 5′-GTG CAC TCC TGG TGT TCT TG-3′ and 5′-ACT CCT GTT TCA CGG TCT GC-3′; for matrix metalloproteinase (MMP)-1, 5′-AAG GCC ACT GGT GAT CTT GC-3′ and 5′-GTT TTC CAG GTA TTT CCA GAC TGT-3′; for MMP-3, 5′-TGG ACA AAG CAG AGC TAC ACA-3′ and 5′-GTG GTG TGT AGT TTA AAA TGC TGT-3′; for MMP-9, 5′-TCT GCC TGC ACC ACT AAA GG-3′ and 5′-CAG GCT GTA CCC TTG GTC TG-3′; for MMP-13, 5′-TTC TGG TCT TCT GGC ACA CG-3′ and 5′-TCC TGG ACC ATA GAG AGA CTG G-3′; and for tissue inhibitor of metalloproteinase-1, 5′-GCC TCC ATC ACT GCT GAT CC-3′ and 5′-GCC CTT ATA ACC AGG TCC GAG-3′.

Collection of GJK data and Gene Ontology (GO) enrichment analysis

The compounds in the five herbs and their related targets were downloaded from the TCMID for further analysis. We screened the targets using STITCH (> 0.7) and performed GO enrichment analysis of the related targets using DAVID Bioinformatics Resources 6.8 with genes of *Rattus norvegicus* as the background. The pathway enrichment analysis of serum metabolism was conducted on the MetaboAnalyst website.

Ultra-performance LC (UPLC)/electrospray ionization (ESI)/Q-TRAP/MS conditions

We conducted LC-MS analysis using an ACQUITY™ UPLC (Waters, USA)/AB 4000 Q-TRAP MS (AB Sciex Pte. Ltd., MA, USA) system and further selected a 2.5 μm Waters XBridge™ BEH C18 analytical column XP (Waters, Torrance, CA) for metabolomics analysis. The injection volume was 10 μL, and the flow rate was set at 0.6 mL/min. Approximately 0.1% formic acid in water (solvent A) and methanol (solvent B) was mixed to be used as a linear gradient mobile phase with a 25 min gradient program. ESI was operated in both positive and negative ion modes with multiple reaction monitoring. The m/z shift was 171.1→125.2 for the internal standard L-phenylalanine-d5 (Phe-d5). In detail, MS conditions were set as follows: an ion spray voltage of ± 4500 V, source

temperature of 450 °C, curtain gas at 20 psi, ion source gas 1 at 40 psi, and ion source gas 2 at 40 psi. Data were further analyzed using the AB Analyst Software (version 1.6.2).

Analysis of the targeted metabolites

Each plasma sample (200 μL) was mixed with 10 mmol/L n-ethylmaleimide (200 μL) in phosphate-buffered saline and methanol (1000 μL). Phe-d5, acting as internal standard, was added to the mixture at 10 ng/mL. After incubation at −20 °C for 20 min, the mixture was centrifuged at 12 000 rpm at 4 °C for 10 min. Then, we evaporated the supernatant under vacuum and obtained a dry residue, which was finally re-dissolved in double-distilled water for UPLC-MS analysis.

We calculated the concentrations of L-tryptophan (Try), 5-hydroxytryptophan (5-HTP), L-kynurenine (Kyn), L-leucine, 5-hydroxytryptamine (5-HT), cholic acid, glutathione disulfide (GSSG), glutathione (GSH), N-phenylacetylglycine, and malondialdehyde in plasma using standard curves, which were obtained from the data tested by standard reference substances (Sigma-Aldrich, St. Louis, MO, USA).

Quality control (QC) samples were prepared from rat plasma, and the endogenous materials in plasma were removed by adding activated charcoal powder (Sigma-Aldrich, MO, USA). QC samples in blank plasma were first verified by UPLC-MS without biomarkers, and QC samples in different concentrations were obtained by dissolving standard solutions of Try, Kyn, 5-HTP, and 5-HT in the blank plasma. Then, data for the eight different concentrations of standard solutions were used to make the standard curves.

Integrated analysis

The integrated analysis of GJK-related targets and metabolites was performed on the MetaboAnalyst website.

Data processing and analysis

We conducted orthogonal projection to latent structures discriminant analysis (OPLS-DA) in SIMCA-P version 14.0 (Umetrics, Umea, Sweden), a software for multivariate statistical analysis, to analyze and rank the metabolites, which could explain most of the variance among groups. Variables were screened by VIP values first, and values exceeding 1 were considered eligible for group discrimination. The selected metabolites were further confirmed by a *t*-test between normal control and disease control with *P* value less than 0.05. Then, the differentially expressed metabolites were analyzed to determine their pathway impact and enrichment in the online software (MetaboAnalyst). A correlation study was also conducted between RA parameters and the metabolites using multiple linear analysis.

The correlation analysis was conducted in SPSS 24. Results were considered statistically significant when the *P* value was less than 0.05.

The data were analyzed using Student's *t*-test and one-way or two-way analysis of variance (ANOVA) followed by Dunnett's *t*-test. The results were considered statistically significant if the *P* value was less than 0.05.

Results

Suppression of AIA in rats by GJK via inhibition of pro-inflammatory cytokines

RA is a systemic disease associated with weight loss and the loss of lean body mass, called rheumatoid cachexia [23]. In this study, we measured the mean body weights of six groups at 11 time points using the AIA rat model (Fig. 2A). The results showed that the body weight in the disease control group decreased significantly beginning on day 15, but GJK (24 g/kg) significantly attenuated the decrease in body weight caused by the development of disease beginning on day 21.

Hind paw volume and arthritis score are the two main methods used to estimate drug effects on clinical arthritis symptoms. Paw swelling of rats was significantly induced after immunization with CFA from day 13 to day 30 compared with the normal group ($P < 0.001$). However, MTX, which is the first-line drug for RA, showed significant inhibitory effects on paw swelling compared with the model group. In the GJK treatment groups, GJK (16 and 24 g/kg) dose-dependently suppressed paw swelling from day 16 to day 30 ($P < 0.001$ or 0.05). Moreover, GJK (24 g/kg) markedly decreased edema, which was similar or better than that observed in the positive control (MTX) group.

The improvement in arthritis scores caused by GJK was consistent with the data for paw volume (Fig. 2C). In the model group, arthritis scores significantly increased from day 13 to day 30 ($P < 0.001$). Among the three GJK groups, 24 g/kg GJK showed optimal effects on the arthritis scores beginning on day 22, and the results of this group were also better than those of the positive control (MTX) group. ESR elevation was significantly suppressed after either MTX or GJK intervention ($P < 0.05$). The highest suppressive effect of GJK against ESR elevation was found at a dose of 24 g/kg (Fig. 2D).

As shown in Fig. 2E, the spleen index markedly increased after CFA induction compared with the normal group ($P < 0.001$). Compared with the disease control group, groups treated with GJK at 24 g/kg had decreased CFA-induced spleen index values. MTX treatment did not show a significant effect.

We also measured the expression levels of pro-inflammatory cytokines using an ELISA kit. The results showed that the expression of TNF-α, IL-1β, IL-6, and IL-17 was significantly stimulated after arthritis induction (Fig. 2F). However, GJK (at 8, 16, and 24 g/kg) dose-dependently inhibited the expression of these cytokines (Fig. 2F). These data suggest significant arthritis symptom relief in AIA rats after 30-day GJK treatment, especially in the 24 g/kg/day group.

Bioinformatics analysis on the drug action targets of GJK using TCMID

To uncover the potential mechanisms of GJK, a bioinformatics analysis approach was used to investigate the targets and pathways of the 358 unique active compounds identified in GJK using TCMID (Supplementary Fig. 1, Supplementary Table 1). Because the mechanism information available was limited, we identified 1749 distinct targets and 745 common targets corresponding to 103 compounds. GO pathway enrichment analyses were performed to explore the general functions and relationships among the 1749 targets using DAVID Bioinformatics Resources 6.8. The 1749 targets were enriched in 165 pathways. Neuroactive ligand–receptor interactions, metabolic pathways, and calcium signaling pathway were the most affected pathways, suggesting that metabolic alterations and bone protection could be the therapeutic targets of GJK and might be associated with multiple target mechanisms in RA treatment. In addition, 14 immune response pathways, including the Toll-like receptor signaling pathway (P = 2.00E-07) and the TNF signaling

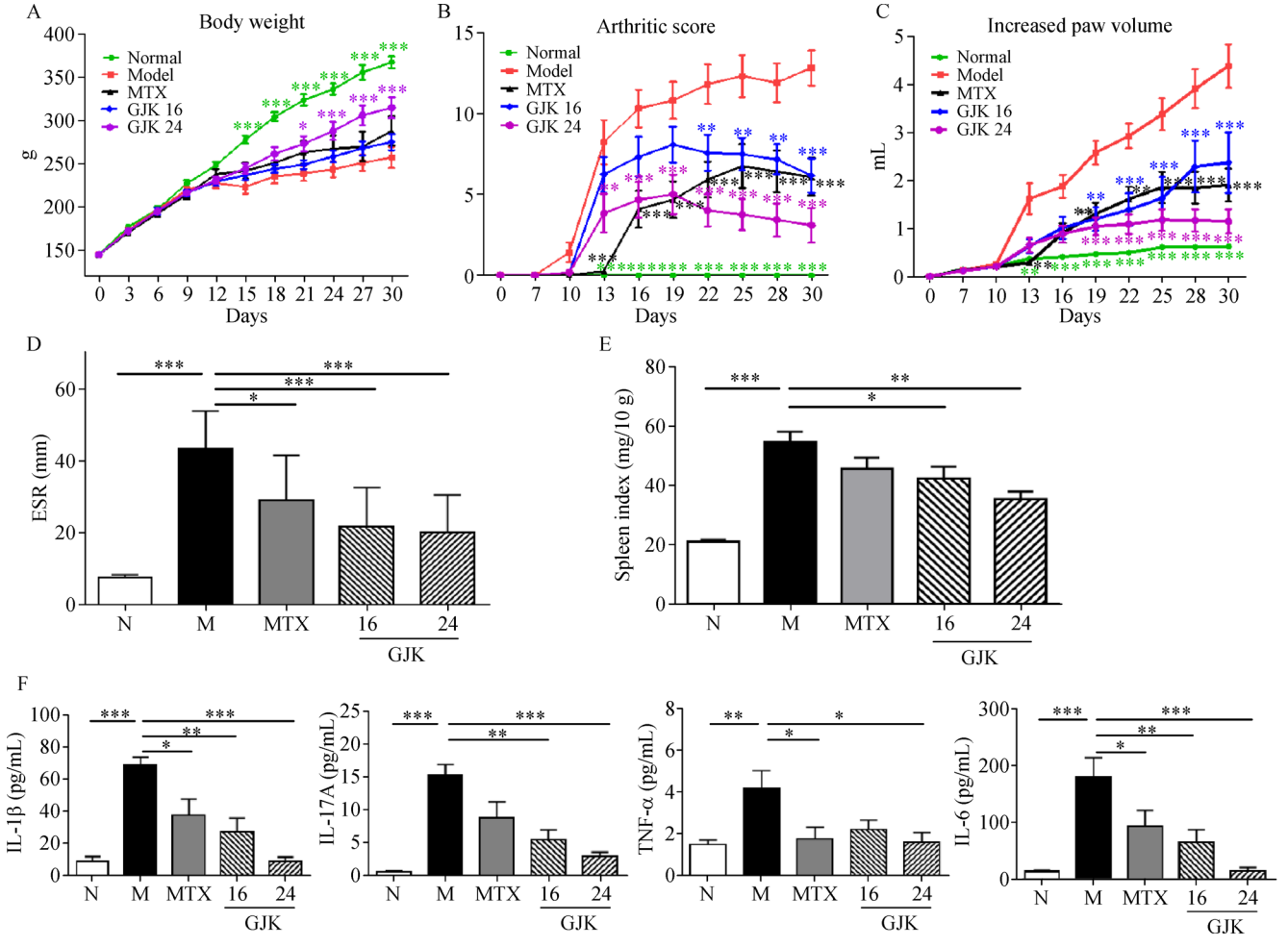

Fig. 2 Pharmacological effects of GJK in AIA rats. Rats were randomly divided into five groups: normal group (N), vehicle disease control group (M), positive control group (MTX), 16 g/kg GJK group, and 24 g/kg GJK group. (A) Changes in body weight in each group (n = 12). (B) Arthritis score changes in the five groups during the 30-day study period (n = 12). (C) Effects of GJK on increased paw volume (n = 12). Group differences in (A), (B), and (C) were analyzed by two-way ANOVA (*P < 0.05, **P < 0.01, ***P < 0.001 vs. model). (D) ESR measurements on the day of sacrifice (n = 11–12). (E) Spleen index assessments in the five groups (n = 12). (F) Effects of GJK on pro-inflammatory cytokine expression (n = 8–12 in IL-1β, IL-17A, and IL-6; n = 5–6 in TNF-α). Group differences in (D), (E), and (F) analyzed by one-way ANOVA (*P < 0.05, **P < 0.01, ***P < 0.001 vs. model).

pathway, were also affected by GJK treatment (Supplementary Table 2). This finding is consistent with the results in Fig. 2F.

Amelioration of bone destruction treated by GJK in AIA rats via suppression of MMP-1, MMP-3, MMP-9, and MMP-13

Axial micro-CT of a rat hind paw is shown in Fig. 3A. Dramatic cortical and trabecular bone loss was evident in the ankle joints, which is characteristic of the AIA disease model. Ankle morphologies were evaluated by 3D reconstruction. The micro-CT radiological images of the paw were used for an overall evaluation of bone damage using CT Analyzer version 1.13 (Supplementary Fig. 2A), but this method could not evaluate very small structures nor provide quantitative results. We found that bone destruction was accurately reflected by reductions in the trabecular BMD, cortical mineral density (tissue mineral density (TMD)), Tb.N, and BV/TV and increases in the porosity percentage in the model group (Supplementary Fig. 2B–2F). These five indicators were closely related to disease status, with an association confidence > 0.5, and facilitated the analysis of bone structure damage from five different perspectives. Here, we combined the data from these five bone destruction indicators to create a composite "micro-CT score." Treatment with MTX or GJK could significantly improve these parameters, especially in the 24 g/kg GJK group. The results showed that the 24 g/kg GJK group exhibited significantly improved bone structure protection (Fig. 3B). Furthermore, 24 g/kg GJK relieved bone damage (i.e., decreased the micro-CT score from severe to mild) (Fig. 3C).

We have found that the targets of GJK compounds enriched in the calcium signaling pathway and GJK revealed well-protective effects on bones. To further explore the underlying mechanism of the bone protection effect of GJK, we investigated gene expression using bone tissue from the upper tibia. As the calcium signaling pathway is associated with RANKL through phosphoinositide-specific phospholipase C [24], we found that the gene expression of osteoclast activation (RANKL/RANK) increased as the OPG/RANKL rate decreased (Fig. 3H) in the GJK-treated groups. Moreover, the expression levels of

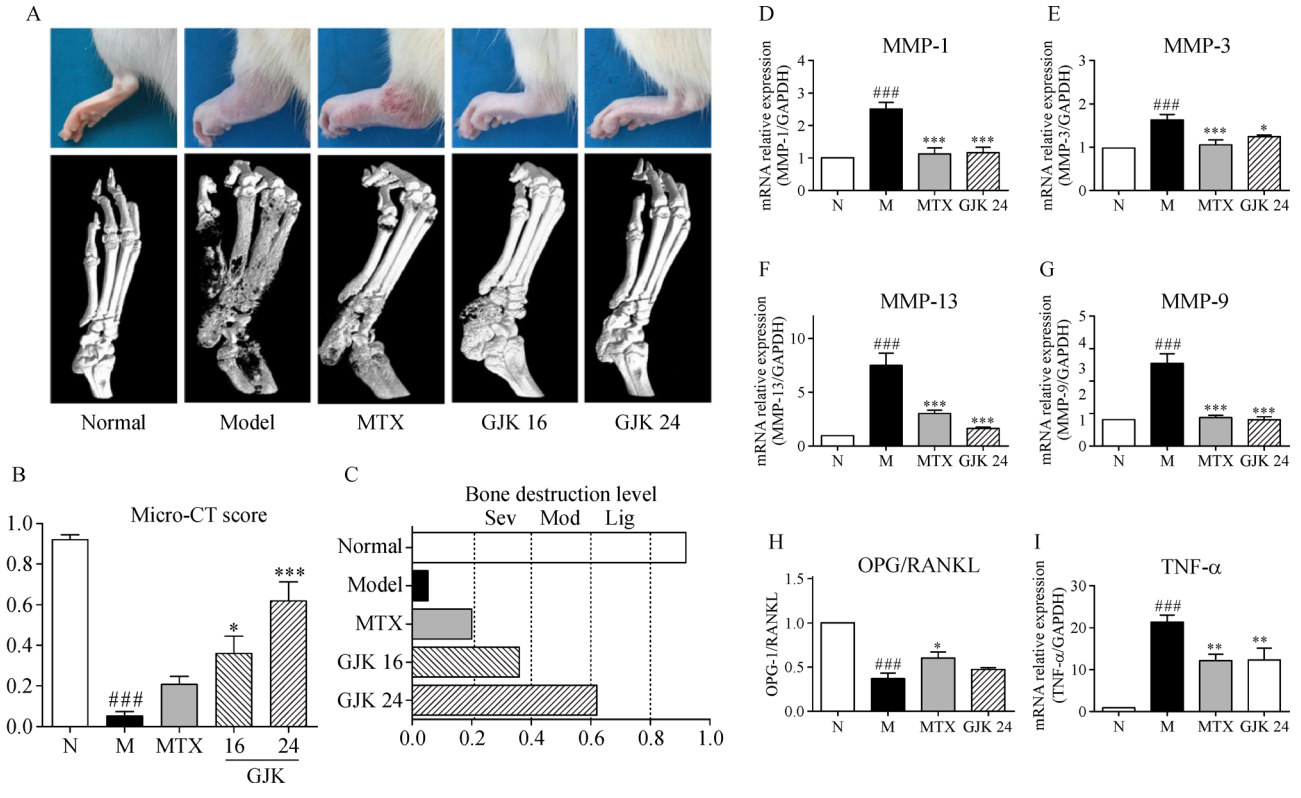

Fig. 3 Bone protective effects of GJK in AIA rats. (A) Representative micro-CT image of the ankles. (B) Inter-group micro-CT score assessments (n = 5–6). (C) Bone destruction level alteration based on micro-CT score. Levels were divided according to micro-CT score. Very severe: 0–0.2; severe: 0.2–0.4; moderate: 0.4–0.6; mild: 0.6–0.8; normal: 0.8–1. (D) MMP-1 mRNA expression of the upper tibia (n = 6). (E) MMP-3 mRNA expression of the upper tibia (n = 5). (F) MMP-13 mRNA expression of the upper tibia (n = 6). (G) MMP-9 mRNA expression of the upper tibia (n = 5). (H) OPG/RANKL rate improvement in the GJK group (n = 5). (I) TNF-α mRNA expression of the upper tibia (n = 5). $^{###}P < 0.001$ vs. control, $^{*}P < 0.05$ vs. model, $^{**}P < 0.01$ vs. model, $^{***}P < 0.001$ vs. model.

MMP-1 (Fig. 3D), MMP-3 (Fig. 3E), MMP-9 (Fig. 3G), and MMP-13 (Fig. 3F) mRNA increased in the disease control group and were significantly downregulated by GJK treatment. Additionally, the gene expression levels of the pro-inflammatory cytokines TNF-α (Fig. 3I), IL-1β, IL-6, and IL-17 (Supplementary Fig. 3) were improved by GJK.

Metabolomics analysis using UPLC-MS/MS

To determine the effects of GJK on metabolic disorder, the metabolic alterations in serum samples from AIA rats were investigated. To validate the stability and repeatability of the method using UPLC-Q-TRAP-MS/MS, we analyzed six injections of identical QC samples. The results showed that peak retention times and areas were less than 1.0% and 5.0%, respectively (Supplementary Fig. 4, Supplementary Tables 3 and 4).

Principal component analysis and OPLS-DA were used to examine the data in a multivariate setting. The AIA model group was different from the normal control group, MTX group, and GJK groups by OPLC-DA (R2X = 0.987, R2Y = 0.992, Q2 = 0.192, n = 8) (Fig. 4A). Statistical analysis revealed 33 potential biomarkers associated with AIA that were responsible for the therapeutic effect of GJK based on VIP > 1.0 in OPLS-DA (Fig. 4B), including 15 upregulated metabolites and 18 downregulated metabolites in the model group compared with those in the normal control group (Fig. 4C). GJK partly corrected the disordered metabolites in AIA to normal levels.

Correlation between the identified metabolites influenced by GJK and RA-associated parameters

To investigate the relationships among RA-associated parameters and the 33 identified metabolites, repeated assessments using correlation analysis were performed on individual metabolites. RA-associated parameters (i.e., weight, arthritis score, paw volume, ESR, and IL-17 expression) were added into the correlation analysis as independent variables, and the levels of the 33 metabolites were set as dependent variables. Seventeen metabolic biomarkers were significantly correlated to the five RA-associated parameters ($P < 0.05$) (Fig. 5). Moreover, the KEGG pathways that mapped these identified 17 metabolites are shown in Supplementary Fig. 5. Results showed

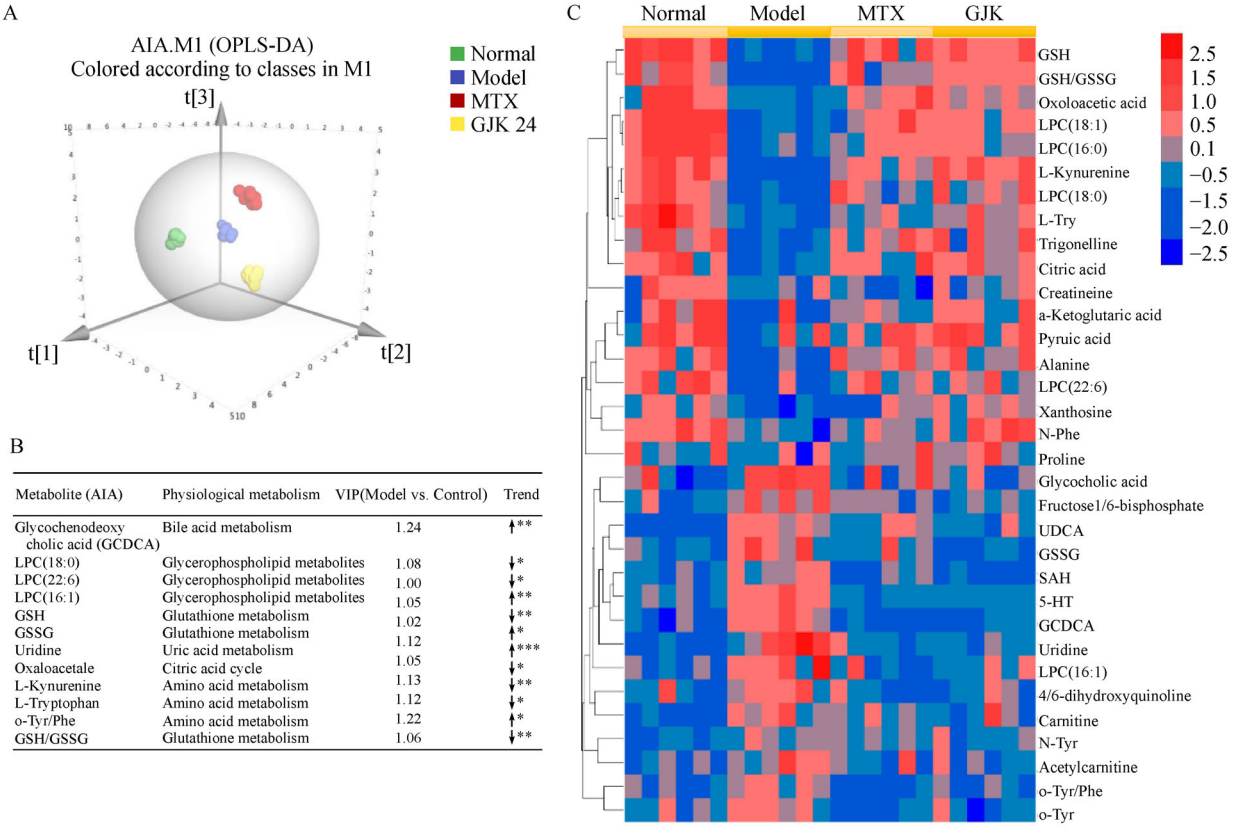

Metabolite (AIA)	Physiological metabolism	VIP(Model vs. Control)	Trend
Glycochenodeoxy cholic acid (GCDCA)	Bile acid metabolism	1.24	↑**
LPC(18:0)	Glycerophospholipid metabolites	1.08	↓*
LPC(22:6)	Glycerophospholipid metabolites	1.00	↓*
LPC(16:1)	Glycerophospholipid metabolites	1.05	↑**
GSH	Glutathione metabolism	1.02	↓**
GSSG	Glutathione metabolism	1.12	↑*
Uridine	Uric acid metabolism	1.05	↑***
Oxaloacetale	Citric acid cycle	1.13	↓*
L-Kynurenine	Amino acid metabolism	1.12	↓**
L-Tryptophan	Amino acid metabolism	1.22	↓*
o-Tyr/Phe	Amino acid metabolism	1.06	↑*
GSH/GSSG	Glutathione metabolism		↓**

Fig. 4 Metabolic alterations in AIA rats. (A) Multiple pattern recognition analysis of plasma biomarkers between normal control group and model group on day 30. OPLS-DA score plot (R2X = 0.987, R2Y = 0.992, Q2 = 0.192, n = 8) of control, model, MTX, and GJK group. (B) Potential biomarkers in response to RA and their metabolic pathways. (C) Potential biomarkers in response to AIA detected by cluster analysis (heatmap).

that these metabolites were mainly associated with glycerophospholipid metabolism, purine metabolism, tryptophan metabolism, GSH metabolism, citric acid cycle, and bile acid biosynthesis pathways.

Modulation of GJK on the metabolism of AIA-associated metabolites

After identifying the 17 metabolites involved in six metabolic pathways, another analysis was conducted to detect the most important metabolic pathways of GJK in AIA. We conducted an integrated analysis of the 1749 targets of 358 compounds in GJK and the 17 AIA-associated metabolites. The results showed that pyruvate metabolism, purine metabolism, and glycolysis were the primary pathways affected by GJK (Fig. 6A, Supplementary Table 5). The levels of uridine and xanthosine in serum were also analyzed. The levels of xanthosine were significantly upregulated, whereas those of uridine were markedly downregulated, indicating that GJK corrects the uric acid metabolism disorder to partly relieve arthritis symptoms (Fig. 6B).

Discussion

TCMs play an important role in the treatment of RA [25].

Many clinical trials using Chinese herbs, Chinese medicine compounds/ingredients, or Chinese medicine decoctions have demonstrated their potential therapeutic effects on RA [13], although their qualities were relatively low. GJK is a modified Chinese herbal formula derived from WTD, which includes Radix Astragali (10 g), Radix Glycyrrhizae (6 g), Radix Paeoniae Alba (12 g), Radix Aconiti Lateralis Praeparata (10 g), and Corydalis Rhizome (10 g). In this study, we evaluated the therapeutic effects of GJK in AIA rats to study the mechanisms of its potential effects on RA. Our results showed that GJK (especially at 24 g/kg) significantly suppressed the severity of arthritis. Based on the "multi-components against multi-targets" theory, we analyzed the herb-related compounds and compound-related targets to explore the underlying mechanisms of GJK. Metabolic pathways and the calcium signaling pathway were identified as the possible pathways by which GJK acts.

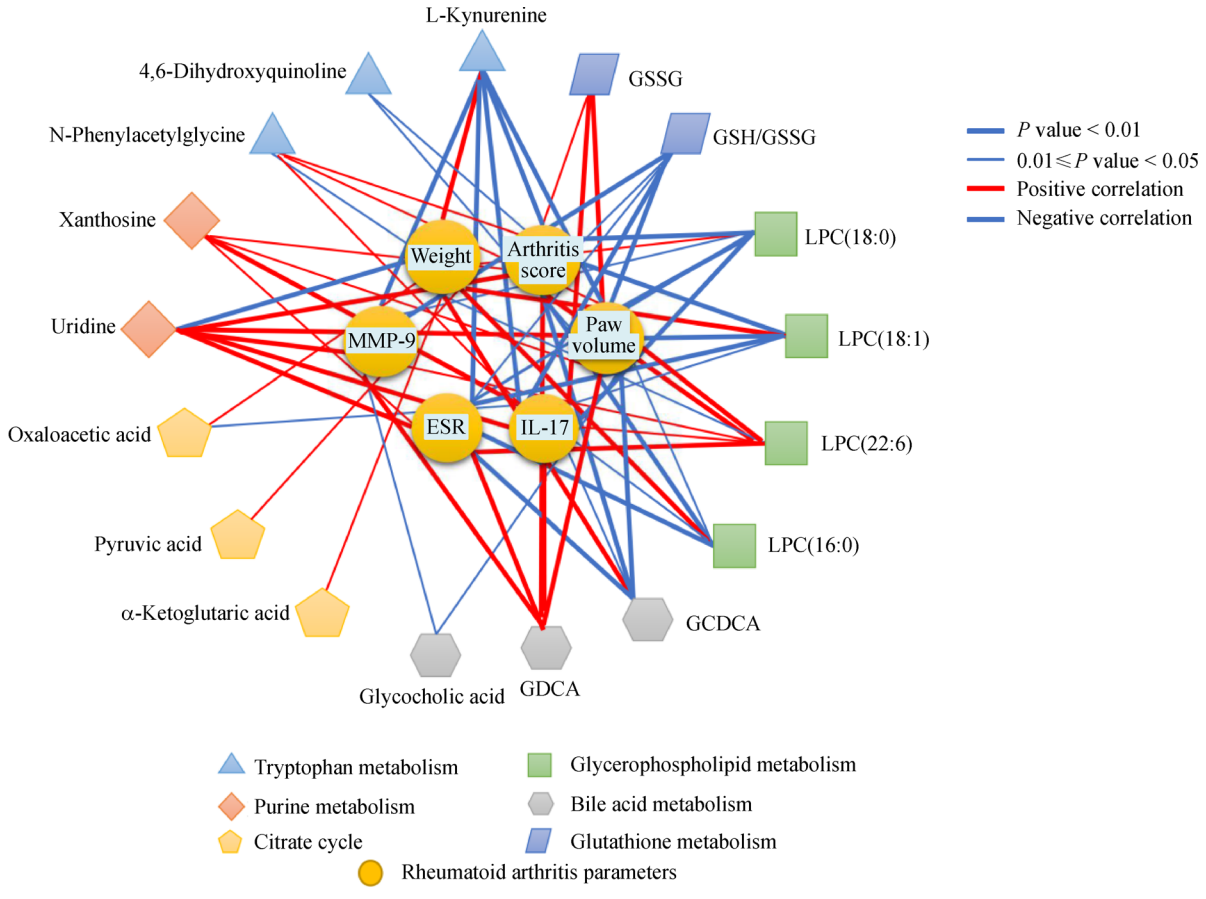

Fig. 5 Correlations between RA parameters and serum metabolite levels with $P < 0.05$ based on correlation analysis. Abbreviation: GSSG, glutathione disulfide; GSH, glutathione; LPC, lysophosphatidylcholine; GDCA, glycodeoxycholic acid; GCDCA, glycochenodeoxycholic acid.

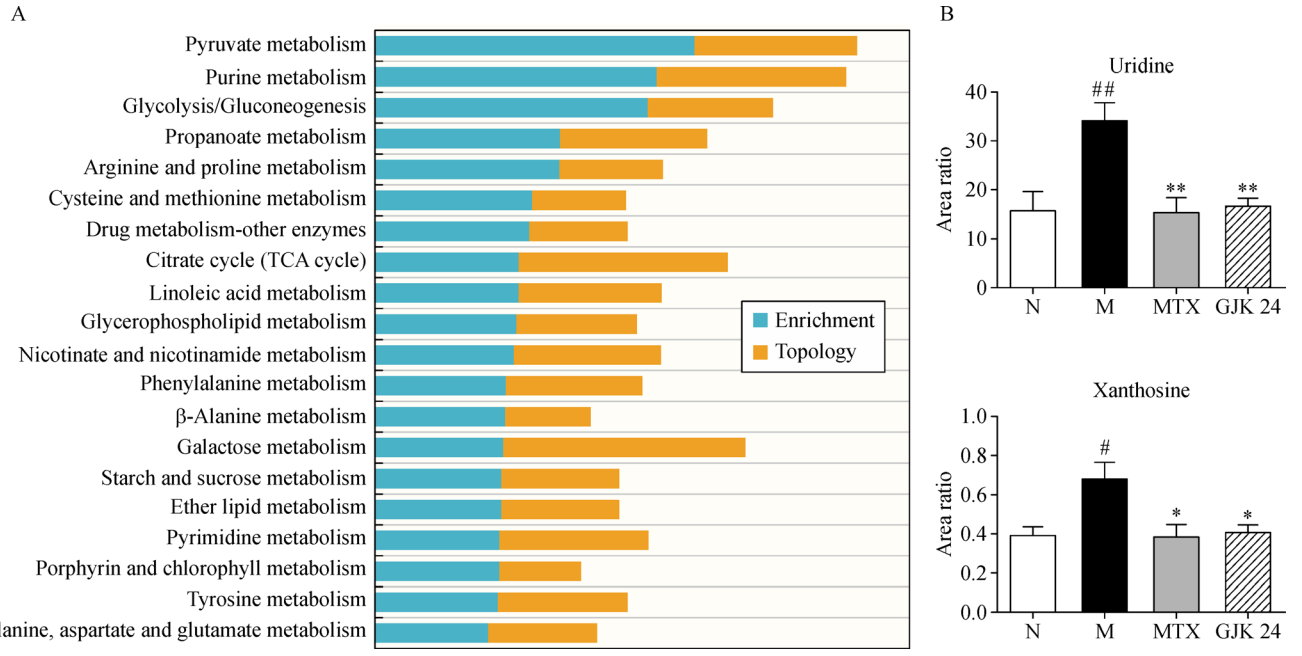

Fig. 6 Effects of GJK on regulating metabolic disorder in AIA rats. (A) Integrated analysis of the targets of GJK and the disease-related metabolites. (B) Quantification of the identified metabolites in serum. $^{\#}P < 0.05$ vs. control, $^{\#\#}P < 0.01$ vs. control, $*P < 0.05$ vs. model, $**P < 0.01$ vs. model.

Calcium signaling is closely related to immune responses [26] and bone metabolism [27]. RANKL–RANK signaling, which is closely related to bone destruction, activates calcium ions (Ca^{2+}) and regulates protein kinase C activation and intracellular Ca^{2+} levels in hematopoietic systems in response to immune receptor stimulation [28]. The compounds in GJK were found to modulate Ca^{2+} signaling pathways, indicating that GJK may affect bone structure remodeling and bone density. We used micro-CT to detect the bone structure and bone density of AIA rats. A new assessment tool, the micro-CT score, was applied in this study to evaluate bone destruction more comprehensively and objectively. Trabecular and cortical bone parameters that quantify the major characteristics of bone pathology were measured with a micro-CT analyzer and combined to quantify bone loss. In addition, the bone damage level was set to illustrate damage. Using this assessment, we found that GJK significantly improves bone damage via bone structure remodeling and bone density enhancement. Modified calcium signaling may also be a mechanism by which GJK protects bones from erosion.

RA is a systemic disease with comorbidities that affect the vasculature, metabolism, and bone [29]. A pre-RA phase lasting for months to years may be characterized by the presence of circulating autoantibodies, increasing concentrations and ranges of inflammatory cytokines and chemokines, and altered metabolism [30]. Metabolic alterations are closely related to the pathogenesis and prognosis of RA [31–33]. In this study, we performed a serum metabolome analysis. OPLS-DA revealed metabolic differences among the normal, model, and GJK groups. We identified 17 metabolites that were significantly correlated with disease severity and may be potential biomarkers that are closely associated with pathogenesis, prognosis, and target treatment. Furthermore, pyruvate metabolism, purine metabolism, and glycolysis were the primary pathways affected by GJK. Pyruvate is the end product of glycolysis [34]. Studies regarding the effects of glycolysis metabolism on RA have demonstrated increased glycolytic activity and autoimmune responses to glycolysis. These results promote new perspectives on the pathogenesis of RA [35,36]. GJK has the potential to regulate the disordered glycolysis to normal, verifying the popular hypothesis that inhibiting the activity of glycolysis could be a means of treating RA. Purine metabolism is also found to be related to the development and prognosis of RA. MTX exerts its anti-arthritic effects via its influence on purine metabolism [37]. Here, we compared GJK's effects on the two metabolites related to purine metabolism pathways, including uridine and xanthosine, to MTX. Results showed that the levels of xanthosine and uridine were synchronously altered by GJK and MTX, indicating a similarity of GJK's anti-arthritis mechanisms to MTX.

GJK is a Chinese formula containing multiple compounds and having multiple targets. In this study, we explored a novel approach to elucidate the complex mechanisms in a complex disease using multiple com-

pound sets, which could help in the *in vivo* identification of multiple targets. We found that metabolism regulation and bone protective effects were significantly associated with the use of GJK in arthritis treatment.

Conclusions

This study identified the underlying mechanisms of GJK using bioinformatics pathway analysis. Based on the bioinformatics results, we confirmed the effects of GJK in metabolic and calcium signaling pathways, which partly explained its therapeutic effect on the RA animal model. Bioinformatics analysis for TCM multiple pathways and multi-omics studies are crucial for analyzing the effects of TCM formulas on treating complex diseases.

Acknowledgements

This work was financially supported by grants from the Macau Science and Technology Development Fund (No. 102/2016/A3).

Compliance with ethics guidelines

Hudan Pan, Yanfang Zheng, Zhongqiu Liu, Zhongwen Yuan, Rutong Ren, Hua Zhou, Ying Xie, and Liang Liu declare that they have no conflicts of interest. All institutional and national guidelines for the care and use of laboratory animals were followed.

Electronic Supplementary Material Supplementary materials are available in the online version of this article at https://doi.org/10.1007/s11684-018-0676-2 and are accessible for authorized users.

References

1. Mikuls TR. Co-morbidity in rheumatoid arthritis. Best Pract Res Clin Rheumatol 2003; 17(5): 729–752
2. Scott DL, Wolfe F, Huizinga TW. Rheumatoid arthritis. Lancet 2010; 376(9746): 1094–1108
3. Gabriel SE. The epidemiology of rheumatoid arthritis. Rheum Dis Clin North Am 2001; 27(2): 269–281
4. Firestein GS. Evolving concepts of rheumatoid arthritis. Nature 2003; 423(6937): 356–361
5. Cooper NJ. Economic burden of rheumatoid arthritis: a systematic review. Rheumatology (Oxford) 2000; 39(1): 28–33
6. Singh JA, Saag KG, Bridges SL Jr, Akl EA, Bannuru RR, Sullivan MC, Vaysbrot E, McNaughton C, Osani M, Shmerling RH, Curtis JR, Furst DE, Parks D, Kavanaugh A, O'Dell J, King C, Leong A, Matteson EL, Schousboe JT, Drevlow B, Ginsberg S, Grober J, St Clair EW, Tindall E, Miller AS, McAlindon T. 2015 American College of Rheumatology Guideline for the Treatment of Rheumatoid Arthritis. Arthritis Rheumatol 2016; 68(1): 1–26
7. Singh JA, Christensen R, Wells GA, Suarez-Almazor ME, Buchbinder R, Lopez-Olivo MA, Ghogomu ET, Tugwell P. Biologics for rheumatoid arthritis: an overview of Cochrane reviews. Sao Paulo Med J 2010; 128(5): 309–310
8. Firestein GS, McInnes IB. Immunopathogenesis of rheumatoid arthritis. Immunity 2017; 46(2): 183–196
9. Koch AE. The pathogenesis of rheumatoid arthritis. Am J Orthop (Belle Mead NJ) 2007; 36(7 Suppl): 5–8
10. Haro I, Sanmartí R. Rheumatoid arthritis: current advances in pathogenesis, diagnosis and therapy. Curr Top Med Chem 2013; 13 (6): 697
11. Wang XR, Su Y, An Y, Zhou YS, Zhang XY, Duan TJ, Zhu JX, Li XF, Wang CH, Wang LZ, Wang YF, Yang R, Wang GC, Lu X, Zhu P, Chen LN, Wang Y, Wang XY, Jin HT, Liu JT, Chen HY, Wei P, Wang JX, Liu XY, Sun L, Cui LF, Shu R, Liu BL, Zhang ZL, Li GT, Li ZB, Yang J, Li JF, Jia B, Zhnag, FX, Tao JM, Lin JY, Wei MQ, Liu XM, Ke D, Hu SX, Ye C, Han SL, Yang XY, Li H, Huang CB, Gao M, Lai P, Song LJ, Mu R, Li ZG. Survey of tumor necrosis factor inhibitors application in patients with rheumatoid arthritis in China. J Peking Univ (Health Sci) (Beijing Da Xue Xue Bao Yi Xue Ban) 2012. 44(2): p. 182–7 (in Chinese)
12. Xu C, Wang X, Mu R, Yang L, Zhang Y, Han S, Li X, Wang Y, Wang G, Zhu P, Jin H, Sun L, Chen H, Cui L, Zhang Z, Li Z, Li J, Zhang F, Lin J, Liu X, Hu S, Yang X, Lai B, Li X, Wang X, Su Y, Li Z. Societal costs of rheumatoid arthritis in China: a hospital-based cross-sectional study. Arthritis Care Res (Hoboken) 2014; 66(4): 523–531
13. Liu J, Sun Y. How does Chinese medicine target cytokine imbalance in rheumatoid arthritis? Chin J Integr Med 2013; 19(11): 874–880
14. Liu J, Chen Z. Traditional Chinese medicine in the new century. Front Med 2011; 5(2): 111–114
15. Xiang Z, Wang X, Liu T, Lv D. Thoughts and exploration on studying pharmacological mechanism of traditional Chinese medicine using network biology approach. China J Chin Materia Medica (Zhongguo Zhong Yao Za Zhi) 2012; 37(2): 146–151 (in Chinese)
16. Wu J, Xie Y, Xiang Z, Wang C, Zhou H, Liu L. Simultaneous determination of multiple components in Guanjiekang in rat plasma via the UPLC-MS/MS method and its application in pharmacokinetic study. Molecules 2016; 21(12): E1732
17. Ma Y, Zhou K, Fan J, Sun S. Traditional Chinese medicine: potential approaches from modern dynamical complexity theories. Front Med 2016; 10(1): 28–32
18. Xue R, Fang Z, Zhang M, Yi Z, Wen C, Shi T. TCMID: traditional Chinese medicine integrative database for herb molecular mechanism analysis. Nucleic Acids Res 2013; 41(Database issue): D1089–D1095
19. Li S, Zhang B. Traditional Chinese medicine network pharmacology: theory, methodology and application. Chin J Nat Med 2013; 11 (2): 110–120
20. Wang C, Xie Y, Xiang Z, Zhou H, Liu L. Simultaneous determination of thirteen major active compounds in Guanjiekang preparation by UHPLC-QQQ-MS/MS. J Pharm Biomed Anal 2016; 118: 315–321
21. Cai X1, Wong YF, Zhou H, Liu ZQ, Xie Y, Jiang ZH, Bian ZX, Xu HX, Liu L. Manipulation of the induction of adjuvant arthritis in Sprague-Dawley rats. Inflamm Res 2006; 55(9): 368–377
22. Zuo J, Xia Y, Li X, Chen JW. Therapeutic effects of dichloromethane fraction of *Securidaca inappendiculata* on adjuvant-induced arthritis in rat. J Ethnopharmacol 2014; 153(2): 352–358

23. Lemmey AB. Rheumatoid cachexia: the undiagnosed, untreated key to restoring physical function in rheumatoid arthritis patients? Rheumatology (Oxford) 2016; 55(7): 1149–1150
24. Komarova SV, Pilkington MF, Weidema AF, Dixon SJ, Sims SM. RANK ligand-induced elevation of cytosolic Ca^{2+} accelerates nuclear translocation of nuclear factor κ B in osteoclasts. J Biol Chem 2003; 278(10): 8286–8293
25. Zhang P, Li J, Han Y, Yu XW, Qin L. Traditional Chinese medicine in the treatment of rheumatoid arthritis: a general review. Rheumatol Int 2010; 30(6): 713–718
26. Hemon P, Renaudineau Y, Debant M, Le Goux N, Mukherjee S, Brooks W, Mignen O. Calcium signaling: from normal B cell development to tolerance breakdown and autoimmunity. Clin Rev Allergy Immunol 2017; 53(2): 141–165
27. Kajiya H. Calcium signaling in osteoclast differentiation and bone resorption. Adv Exp Med Biol 2012; 740: 917–932
28. Negishi-Koga T, Takayanagi H. Ca^{2+}-NFATc1 signaling is an essential axis of osteoclast differentiation. Immunol Rev 2009; 231 (1): 241–256
29. Leah E. Rheumatoid arthritis. Assessment of CVD in patients with RA by strain imaging. Nat Rev Rheumatol 2013; 9(9): 506
30. Paul BJ, Kandy HI, Krishnan V. Pre-rheumatoid arthritis and its prevention. Eur J Rheumatol 2017; 4(2): 161–165
31. da Cunha VR, Brenol CV, Brenol JC, Xavier RM. Rheumatoid arthritis and metabolic syndrome. Rev Bras Reumatol 2011; 51(3): 260–268
32. Chang X, Wei C. Glycolysis and rheumatoid arthritis. Int J Rheum Dis 2011; 14(3): 217–222
33. Yang Z, Shen Y, Oishi H, Matteson EL, Tian L, Goronzy JJ, Weyand CM. Restoring oxidant signaling suppresses proarthritogenic T cell effector functions in rheumatoid arthritis. Sci Transl Med 2016; 8(331): 331ra38
34. Gray LR, Tompkins SC, Taylor EB. Regulation of pyruvate metabolism and human disease. Cell Mol Life Sci 2014; 71(14): 2577–2604
35. Perl A. Review: Metabolic control of immune system activation in rheumatic diseases. Arthritis Rheumatol 2017; 69(12): 2259–2270
36. Weyand CM, Goronzy JJ. Immunometabolism in early and late stages of rheumatoid arthritis. Nat Rev Rheumatol 2017; 13(5): 291–301
37. Cronstein BN. Low-dose methotrexate: a mainstay in the treatment of rheumatoid arthritis. Pharmacol Rev 2005; 57(2): 163–172